Journal of Sound and Vibration (1999) **225**(3), 425–446
Article No. jsvi.1999.2184, available online at http://www.idealibrary.com on IDEAL®

MODE IDENTIFICATION FOR ROTATING RIGID SHAFT WITH FLEXIBLE DISKS BY MODE SPLITS

CHONG-WON LEE, JONG-SEOK HAM

Center for Noise and Vibration Control (NOVIC), Department of Mechanical Engineering, KAIST, Science Town, Taejon 305-701, *South Korea*

(*Received* 31 *August* 1998, *and in final form* 12 *January* 1999)

This paper investigates the mode splits of the bending coupled modes of a rotating shaft with multiple flexible disks, in which the disks are rigidly attached to the rigid shaft supported by bearings. The bending coupled modes, in which shaft bending modes are coupled with one nodal diameter disk modes, are classified as the balanced and unbalanced modes. The mode splits of the balanced modes are the same as those of pure disk modes since the shaft does not experience any motion. On the other hand, the mode splits between pairs of the forward and backward unbalanced modes are found to be dependent upon the disk/shaft configuration and the shaft support stiffness, as well as the rotational speed and the ratio of polar to diametrical moment of inertia.

1. INTRODUCTION

The trend toward high performance and efficiency in the design of rotating machines, such as computer disk memory, gas turbines and grinding wheels, has required the need to consider the flexibility of disks for accurate analysis of their vibrational characteristics. However, due to the dynamic coupling between shaft and disks of a rotating shaft-multiple disk, the vibration analysis becomes very complicated.

In the area of rotor dynamics, the vibration characteristics of a shaft–disk system have been studied by many investigators, and the studies are mainly concerned with the effects of disk flexibility on the shaft whirl and vibration [1–6]. Some other studies [7, 8] discussed the importance of the coupling between disk and shaft, and the focus was both on disk and shaft motion. However, the analysis model, which consists of flexible shaft and disks, was so complicated that the coupling between the disk and shaft was not clearly understood.

The vibration and stability analysis of rotating disks such as grinding wheels, circular saws, wafer cutting machines, and computer disk memory units has been of great interest to many researchers [9–15]. Among such studies, the presence of backward and forward travelling wave modes in a rotating disk has been extensively investigated in the literature [13–15]. Chen and Bogy [16] presented

0022-460X/99/330425 + 22 $30.00/0

a theoretical study to predict the effect of parameter change on the eigenvalues of the system in which a spinning disk contacts with a stationary load system. However, these studies [9–16] did not take into consideration the support motion in their analysis models. Recently, some studies have been carried out, which considered not only disk vibration but also support motion. Mote [17], Yang [18], and Chen and Bogy [19] took into consideration the rigid body motion in a single-disk system for their analysis. Shen and Ku [20, 21] investigated the multiple elastic disks–spindle system which undergoes rigid-body rotation (rocking) and axial translation. They referred the lower precessional modes as unbalanced modes, and the disk modes as balanced modes of the disk–shaft system.

Here, we can classify coupled vibration modes of a multiple disks–shaft system into bending coupled and axially coupled modes: the former is associated with disk modes with one nodal diameter and the angular moment caused by elastic deformation of disks affects the shaft motion, whereas the latter is associated with the disk modes with no nodal diameter and the axial force caused by elastic deformation of disks. We also classify the bending and axially coupled modes into balanced and unbalanced modes. Hereafter, we mean bending coupled modes when we mention balanced or unbalanced modes without any special notation. The balanced $(m, 1)$ modes or the balanced modes associated with $(m, 1)$ disk mode, where the first and second indices in parenthesis denote the number of nodal circle and diameter of disk, lead to pure disk modes since the total angular momentum caused by $(m, 1)$ disk modes, $m = 0, 1, 2, \ldots$, is kept at zero. The unbalanced $(m, 1)$ modes couple the shaft precessional mode with disk modes, in which the angular momentum caused by the disk elastic mode allows the shaft to have a precessional mode. The unbalanced modes will also be classified as forward and backward unbalanced modes according to the precessional direction.

This paper studies the dynamics of a rotating shaft with multiple flexible disks, especially the effect of disk flexibility on the mode split of the bending coupled modes over the rotational speed, by which the modal parameters can be easily identified by using a waterfall plot of experimental results. Without the knowledge of vibrational characteristics of this system, it is very difficult to identify the modal parameters by the conventional modal testing method utilizing mode shapes, since the shaft and disk motions are coupled with each other and their modes tend to be closely packed in the frequency domain. In addition, it frequently occurs that the vibration signal of the rotational part cannot be obtained and pick-ups cannot be placed properly due to space limitation.

The splits of each forward and backward unbalanced mode pair over rotational speed are investigated by introducing parameters such as the coupling factor, the ratio of polar to diametrical moment of inertia and the shaft support stiffness. The characteristic equation of motion is derived and discretized by employing single- or two-mode approximation, to solve for the natural frequencies associated with the unbalanced modes. Although the analysis model assumes that the shaft is rigid, the analytical findings can be easily extended to account for flexibility of the shaft. The mode splits of the axially coupled modes are not investigated since such modes do not split as the rotational speed increases.

2. EQUATIONS OF MOTION

The typical commercial HDD spindle system shown in Figure 1 is essentially an assemblage of a shaft with multiple disks and support bearings, which is normally modelled as in Figure 2. The motion of a multiple disks–shaft system can be conveniently described with four co-ordinate frames: the inertial reference frame $X_0\,Y_0\,Z_0$ of which the X_0-axis is located on the centerline of bearings, the reference frame XYZ which is parallel to the inertial frame but with its origin on the shaft

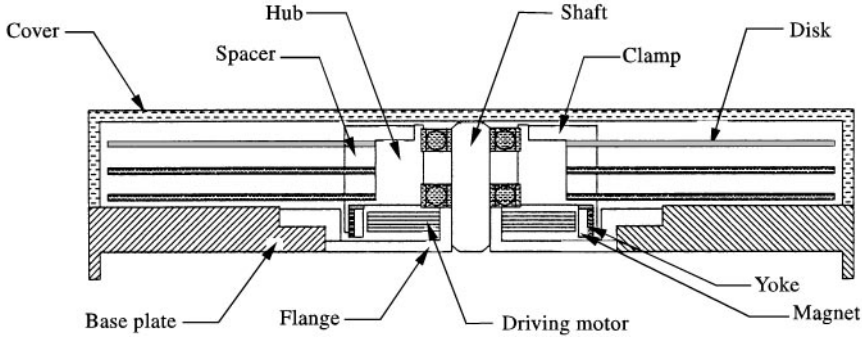

Figure 1. Schematic diagram of a typical three-disk HDD spindle system [22].

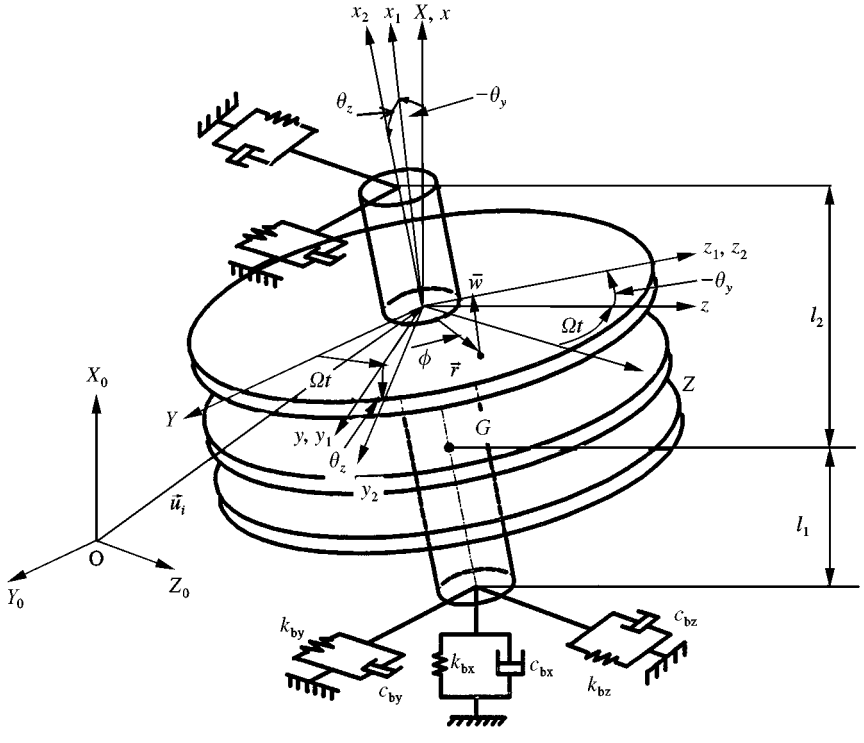

Figure 2. Analysis model and the co-ordinate system.

centerline or the disk center, the local frame xyz which rotates with the shaft about the X-axis and the local frame $x_2y_2z_2$ which moves with the rigid-body motion of the disk. The orientation of the $x_2y_2z_2$ frame is defined by rotation of $-\theta_y$ about the y-axis and then rotation of θ_z about the z_2-axis. Assuming that the disks behave according to the classical plate theory and using Hamilton's principle, we can derive the equations of motion in the rotating frame (xyz) with its origin located at the centroid of the multiple disks–shaft system as given in Appendix A, which are essentially identical to the derivations made in references [8, 21]. When the bearings are isotropic and the resultant moment of the bearing forces with respect to the centroid of the system is zero, the rotary and translational motions of the shaft become uncoupled. In addition, the equations of motion can be discretized by use of Galerkin's method or the variational form of the equation of motion given in Appendix A, in which the elastic motion of the ith disk is expressed as

$$w^{(i)}(r, \phi, t) = \sum_{m,n=0}^{\infty} R_{mn}^{(i)}(r)\{a_{mn}^{(i)}(t)\cos n\phi + b_{mn}^{(i)}(t)\sin n\phi\}, \tag{1}$$

where m and n are the number of nodal circles and nodal diameters of the disk respectively, $R_{mn}^{(i)}(r)$ is the radial mode shape of the disk, and $a_{mn}^{(i)}(t)$ and $b_{mn}^{(i)}(t)$ are the co-ordinates to be determined. Since it holds that

$$\int_0^{2\pi} \sin\phi\cos n\phi = \int_0^{2\pi} \cos\phi\sin n\phi = 0$$

and

$$\int_0^{2\pi} \sin\phi\sin n\phi = \int_0^{2\pi} \cos\phi\cos n\phi = \begin{cases} 0 & \text{for } n \neq 1, \\ \pi & \text{for } n = 1, \end{cases} \tag{2}$$

it can be easily proven that the disk modes with one nodal diameter couple with the rotary motion of the shaft, the disk modes with no nodal diameter couple with the axial motion of the shaft, and the disk modes with more than one nodal diameter do not couple with the other modes [8, 21].

Considering only the one nodal diameter modes of N disks and introducing the complex co-ordinates in the rotating frame defined as

$$\psi = \theta_z + \mathrm{j}\theta_y,\ c_{m1}^{(i)} = a_{m1}^{(i)} + \mathrm{j}b_{m1}^{(i)}, \quad i = 1, 2, \ldots, N, \tag{3}$$

we can obtain the discretized equations of bending coupled motion as

$$\begin{gathered} J_T\{\ddot{\psi} - \mathrm{j}\Omega(\alpha - 2)\dot{\psi} + (\alpha - 1)\Omega^2\psi + \omega_t^2\psi\} - \sum_i \sum_m B_{m1}^{(i)}(\ddot{c}_{m1}^{(i)} + \Omega^2 c_{m1}^{(i)}) = 0, \\ A_{m1}^{(i)}\{\ddot{c}_{m1}^{(i)} + \omega_{m1c}^{(i)^2} c_{m1}^{(i)}\} - B_{m1}^{(i)}(\ddot{\psi} + \Omega^2\psi) = 0, \\ A_{m1}^{(i)} = \pi\rho_d h\int_{(i)} R_{m1}^{(i)^2}(r) r\,\mathrm{d}r, \quad B_{m1}^{(i)} = \int_{(i)} \pi\rho_d h R_{m1}^{(i)}(r) r^2\,\mathrm{d}r, \quad \omega_t^2 = \frac{k_t}{J_T}. \end{gathered} \tag{4}$$

Here, ρ_d and h are the density and thickness of the disk, k_t is the shaft support stiffness, J_T is the total diametrical moment of inertia, α is the ratio of the polar to the diametrical moment of inertia for the system, $R_{m1}^{(i)}$ is the radial mode shape in

the presence of centrifugal effect, $\omega_{m1c}^{(i)}$ is the natural frequency defined in the rotating frame of the rotating disk subject to the in-plane centrifugal force, and Ω is the rotational speed. The above equations may easily be re-expressed in the stationary co-ordinates by using the co-ordinate transformation relations given by

$$\tilde{\psi} = \psi e^{j\Omega t}, \quad \tilde{c}_{m1}^{(i)} = c_{m1}^{(i)} e^{j\Omega t}, \tag{5}$$

where $\tilde{\psi}$ and $\tilde{c}_{m1}^{(i)}$ are the complex stationary co-ordinates. Since it holds for the shaft with N identical disks that for $m = 0, 1, 2, \ldots, M$, and $i = 1, 2, \ldots, N$,

$$R_{m1}^{(i)} = R_{m1}, \qquad \omega_{m1c}^{(i)} = \omega_{m1c}, \qquad A_{m1}^{(i)} = A_{m1}, \qquad B_{m1}^{(i)} = B_{m1},$$

equation (4) becomes [20, 21]

$$[M]\{\ddot{q}\} + jJ_T\Omega[G]\{\dot{q}\} + [K]\{q\} = \{0\}, \tag{6}$$

$$\{q\} = [\psi \quad c_{01}^{(1)} \quad c_{01}^{(2)} \quad \cdots \quad c_{M1}^{(N)}]^T, \tag{7}$$

$$[M] = \begin{bmatrix} J_T & -B_{01} & -B_{01} & \cdots & -B_{M1} \\ -B_{01} & A_{01} & 0 & \cdots & 0 \\ -B_{01} & 0 & A_{01} & \cdots & 0 \\ \vdots & \vdots & \vdots & \ddots & \vdots \\ -B_{M1} & 0 & 0 & 0 & A_{M1} \end{bmatrix}, \quad [G] = \begin{bmatrix} 2-\alpha & 0 & 0 & \cdots & 0 \\ 0 & 0 & 0 & \cdots & 0 \\ 0 & 0 & 0 & \cdots & 0 \\ \vdots & \vdots & \vdots & \ddots & \vdots \\ 0 & 0 & 0 & \cdots & 0 \end{bmatrix},$$

$$[K] = \begin{bmatrix} J_T\{\omega_t^2 + (\alpha-1)\Omega^2\} & -B_{01}\Omega^2 & -B_{01}\Omega^2 & \cdots & -B_{M1}\Omega^2 \\ -B_{01}\Omega^2 & A_{01}\omega_{01c}^2 & 0 & \cdots & 0 \\ -B_{01}\Omega^2 & 0 & A_{01}\omega_{01c}^2 & \cdots & 0 \\ \vdots & \vdots & \vdots & \ddots & \vdots \\ -B_{M1}\Omega^2 & 0 & 0 & \cdots & A_{M1}\omega_{M1c}^2 \end{bmatrix}, \tag{8}$$

where the subscript M is the number of one nodal diameter modes of interest. If we set

$$[\psi \quad c_{01}^{(1)} \quad c_{01}^{(2)} \quad \cdots \quad c_{M1}^{(N)}]^T = [\Psi \quad C_{01}^{(1)} \quad C_{01}^{(2)} \quad \cdots \quad C_{M1}^{(N)}]^T e^{st}, \tag{9}$$

we obtain, from equation (6),

$$\begin{bmatrix} E & -B_0 & -B_0 & \cdots & -B_m & -B_m & \cdots & -B_M \\ -B_0 & A_0 & 0 & & 0 & 0 & & 0 \\ -B_0 & 0 & A_0 & & 0 & 0 & & 0 \\ \vdots & & & \ddots & & & & \vdots \\ -B_m & 0 & 0 & & A_m & 0 & & 0 \\ -B_m & 0 & 0 & & 0 & A_m & & 0 \\ \vdots & & & & & & \ddots & \\ -B_M & 0 & 0 & \cdots & 0 & 0 & & A_M \end{bmatrix} \begin{Bmatrix} \Psi \\ C_{01}^{(1)} \\ C_{01}^{(2)} \\ \vdots \\ C_{m1}^{(1)} \\ C_{m1}^{(2)} \\ \vdots \\ C_{M1}^{(N)} \end{Bmatrix} = \{0\}, \tag{10}$$

where

$$E = J_T\{s^2 + j\Omega(2-\alpha)s + \omega_t^2 + (\alpha-1)\Omega^2\},$$

$$A_m = A_{m1}\cdot(s^2 + \omega_{m1c}^2) = \int \pi\rho_d h R_{m1}^2 r\,\mathrm{d}r(s^2 + \omega_{m1c}^2), \tag{11a–c}$$

$$B_m = B_{m1}\cdot(s^2 + \Omega^2) = \int \pi\rho_d h R_{m1} r^2\,\mathrm{d}r(s^2 + \Omega^2).$$

The characteristic equation associated with equation (10) becomes

$$(EA_0A_1\cdots A_M - NB_0^2A_1\cdots A_M - NB_1^2A_0A_2\cdots A_M - \cdots)(A_0A_1\cdots A_2A_M)^{N-1} = 0. \tag{12}$$

From equation (12), Shen and Ku [20, 21] introduced the concept of "balanced and unbalanced" modes of a multiple elastic disk system, but treated only the first unbalanced modes [refer to Figure 3(a)] in addition to the balanced modes. In this case, the unbalanced (m, 1) mode pair is the ($m+1$)th unbalanced mode pair which is associated with the m nodal circle and one nodal diameter mode of disk. The solution to the relation

$$(A_0A_1A_2\cdots A_M)^{N-1} = 0 \tag{13}$$

leads to the balanced modes of the disks: while the shaft experiences no motion, the disks experience the balanced elastic deformations so that the total angular momentum is kept at zero. Another solution to the relation

$$EA_0A_1\cdots A_M - NB_0^2A_1\cdots A_M - NB_1^2A_0A_2\cdots A_M - \cdots = 0 \tag{14}$$

implies that the shaft and disks experience in-phase or out-of-phase rotary motions with each other, while the disks behave like a single disk, as shown in Figure 3. Thus, the multiple disks–shaft system can be described by a pure disk system for the balanced case, and by a single disk–shaft system for the unbalanced case. The characteristic equation (14) for the unbalanced modes can be written as

$$\{s^2 - j\Omega(\alpha-2)s + \omega_t^2 + (\alpha-1)\Omega^2\}\prod_{m=0}^{M}(s^2+\omega_{m1c}^2) - F_0(s^2+\Omega^2)^2\prod_{m=1}^{M}(s^2+\omega_{m1c}^2)$$
$$- F_1(s^2+\Omega^2)^2\prod_{m=0,m\neq 1}^{M}(s^2+\omega_{m1c}^2) - F_2(s^2+\Omega^2)^2\prod_{m=0,m\neq 2}^{M}(s^2+\omega_{m1c}^2) - \cdots = 0. \tag{15}$$

Here the coupling factor F_m is defined as

$$F_m = \frac{N\pi\rho_d h}{J_T}\frac{[\int_{r_1}^{r_2} R_{m1}(r)r^2\,\mathrm{d}r]^2}{\int_{r_1}^{r_2} R_{m1}^2(r)r\,\mathrm{d}r} = \frac{N\pi\rho_d h}{J_T}\frac{r_2^4[\int_{\xi_1}^{1} R_{m1}(\xi)\xi^2\,\mathrm{d}\xi]^2}{\int_{\xi_1}^{1} R_{m1}^2(\xi)\xi\,\mathrm{d}\xi} = \eta H_m, \tag{16}$$

$$H_m = \frac{[\int_{\xi_1}^{1} R_{m1}(\xi)\xi^2\,\mathrm{d}\xi]^2}{\int_{\xi_1}^{1} R_{m1}^2(\xi)\xi\,\mathrm{d}\xi}, \quad \eta = \frac{N\pi\rho_d h r_2^4}{J_T}, \quad \xi = \frac{r}{r_2}, \tag{17}$$

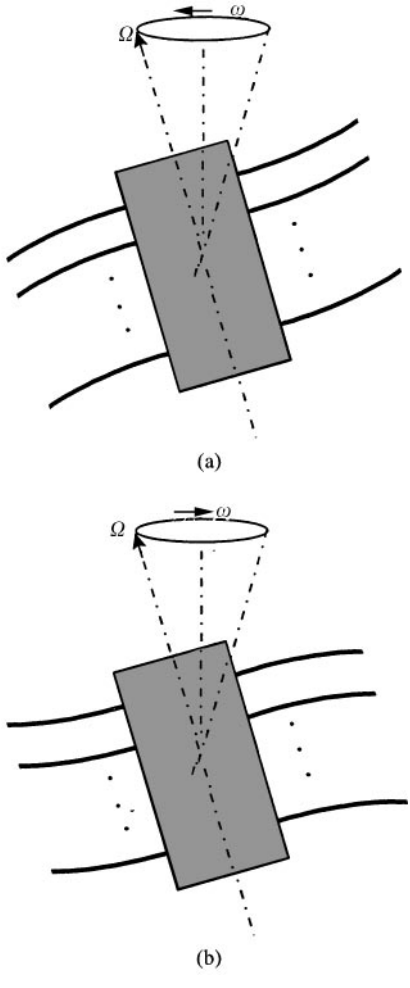

Figure 3. Examples of unbalanced (0, 1) modes: (a) in-phase (first) forward precessional unbalanced (0, 1) mode; (b) out-of-phase (second) backward precessional unbalanced (0, 1) mode. ω is the precessional speed and Ω is the rotational speed.

where r_1 and r_2 are the inner and outer radii of the disk respectively. Here H_m and η will be referred to as the disk flexibility factor and the configuration factor respectively.

3. ANALYSIS OF PARAMETERS

From equation (15), we can obtain the natural frequencies of the unbalanced modes, as the rotational speed is varied, for given parameters associated with a multiple disks–shaft system. It should be noted that two kinds of uncoupled basic motions, which are the pure disk vibration and the rotary motion of a simple gyroscopic system, are coupled with each other through the coupling terms associated with $F_m = \eta H_m$, $m = 0, 1, 2, \ldots, M$. The disk flexibility factor H_m depends only on the ratio of inner and outer radii and the dimensionless radial

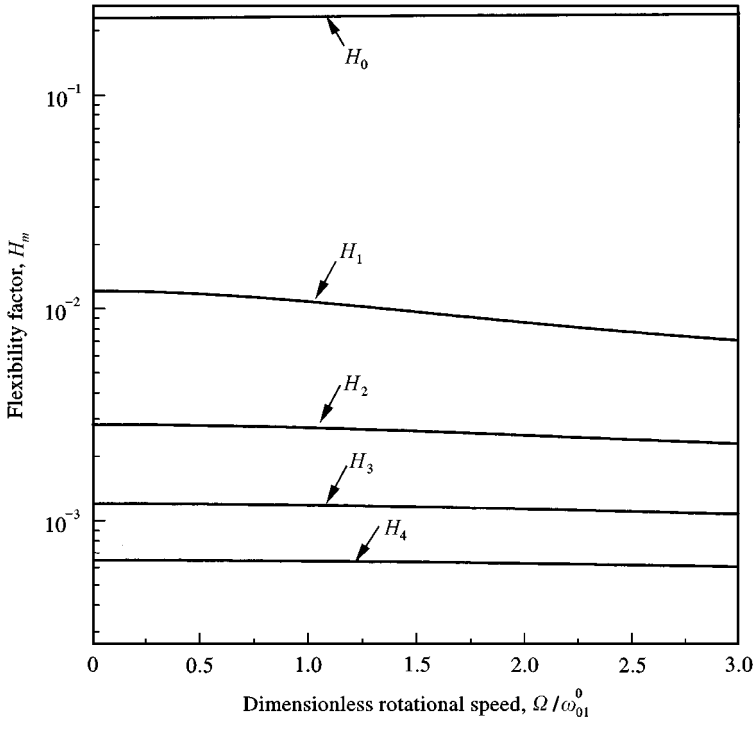

Figure 4. Flexibility factor (H_m) for the five lowest modes with one nodal diameter of a rotating disk: $\xi_1 = 0{\cdot}316$, $\omega^0_{01} = 597$ Hz.

mode shape of the disk, which is a function of the dimensionless rotational speed and the boundary conditions as shown in Appendix B.

Figure 4 shows the disk flexibility factor H_m for the five lowest modes with one nodal diameter as the rotational speed is varied. The numerical calculations were carried out by adopting the finite-element method using annular finite-element [24]. Note that the disk flexibility factor drastically decreases as the number of nodal circles increases, whereas it remains almost unchanged as the rotational speed increases. It implies that the one nodal diameter modes with more than one nodal circle do not significantly contribute to the coupling with the shaft rotary mode and the centrifugal force caused by change in the rotational speed has an insignificant influence on the radial mode shapes. Therefore, it suggests that one mode or, at most, two mode approximation is enough to calculate the natural frequencies of HDD spindle systems with fair accuracy.

Figure 5 shows the disk flexibility factor H_0 associated with the one nodal diameter and no nodal circle mode of the disk as the clamping ratio of the disks is varied. Note that the factor H_0 significantly increases as the clamping ratio of the disk decreases, implying that the corresponding radial mode shape is influenced greatly by change in the clamping ratio. When the clamping ratio approaches zero, the flexibility factor approaches the maximum value of 0·25. On the other hand, when the clamping ratio is near 1, it decreases to zero and the coupling effect vanishes.

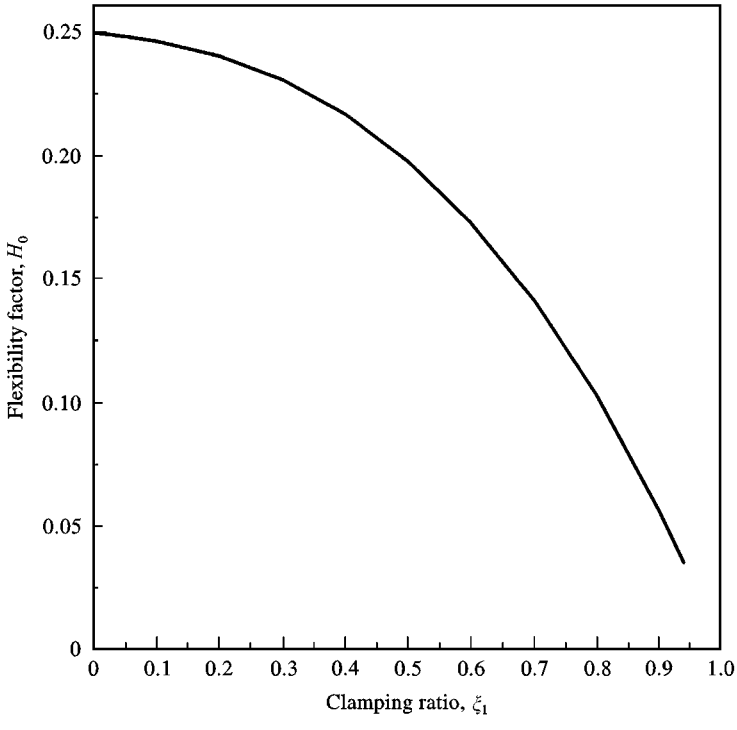

Figure 5. Flexibility factor (H_0) for (0, 1) mode of a non-rotating disk with the clamping ratio varied.

TABLE 1

Parameters for a shaft with disks equally and symmetrically spaced between 26 *mm shaft length*: *shaft length* = 30 *mm*, *shaft outer radius* = 15 *mm*, *shaft inner radius* = 8 *mm*, *disk outer radius* = 47·5 *mm*, *disk inner radius* = 15 *mm*, *disk thickness* = 8 *mm*

Number of disks	$J_P(\times 10^{-6})$ kg m^2	$J_T(\times 10^{-6})$ kg m^2	χ_1	χ_2	α	η
0	6·14	6·26	—	—	0·98	0
1	23·87	15·12	0·71	0·35	1·58	2·37
2	41·61	23·99	0·35	0·17	1·73	2·99
3	59·34	32·86	0·24	0·12	1·81	3·27
5	94·81	50·60	0·14	0·07	1·87	3·54
10	183·48	94·93	0·07	0·03	1·93	3·77

Note: Gap between two neighboring disks is equal to 26 mm divided by the number of disks minus the thickness of disk.

The configuration factor η, which determines the coupling factor together with the disk flexibility factor, depends on the thickness and the outer radius of the disks, the number of disks and the diametrical moment of inertia of the assembled system. The configuration factor η and the ratio α of polar to diametrical moment of inertia

can be rewritten as

$$\eta = \frac{N\pi\rho_d h r_2^4}{\sum_i^N J_T^{(i)} + J_T^s} = \frac{N\pi\rho_d h r_2^4}{NJ_T^d + \Delta + J_T^s} = \frac{\pi\rho_d h r_2^4}{J_T^d(1+\chi_1)}, \tag{18}$$

$$\alpha = \frac{\sum_i J_p^{(i)} + J_p^s}{\sum_i J_T^{(i)} + J_T^s} = \frac{NJ_p^d + J_p^s}{NJ_T^d + \Delta + J_T^s} = \frac{J_p^d(1+\chi_2)}{J_T^d(1+\chi_1)}, \tag{19}$$

$$\chi_1 = \frac{\Delta + J_{\mathrm{T}}^s}{NJ_T^d}, \quad \chi_2 = \frac{J_p^s}{NJ_p^d}, \tag{20}$$

where $J_T^{(i)}$ is the diametrical moment of inertia of the ith disk with respect to its own axis, and Δ is the shifting effect because the moments of inertia are to be calculated with respect to the axes located at the centroid of the system. In general, since the value α is smaller for the shaft than for the disk, χ_1 is larger than χ_2. Table 1 illustrates the parameter values for a shaft with multiple disks which are equally spaced and symmetrically arranged with respect to its centroid. Note that as the number of disks increases, both α and η tend to increase as expected. For given parameters α, η and H_m, equation (15) can be solved to obtain natural frequencies for a shaft with multiple disks. The ranges that H_m and η can take are given in equations (C1) and (C3) in Appendix C.

4. MODE SPLIT

In case of rigid disk, since ω_{m1c} goes to infinity, equation (15) reduces to, in the rotating frame,

$$s^2 - \mathrm{j}\Omega(\alpha - 2)s + \omega_t^2 + (\alpha - 1)\Omega^2 = 0 \tag{21}$$

or, equivalently in the stationary frame, by replacing s by $s - \mathrm{j}\Omega$,

$$s^2 - \mathrm{j}\Omega\alpha s + \omega_t^2 = 0. \tag{22}$$

As shown in Figure 6, it is well known [23] that the split in absolute frequency between the forward and backward precessional modes of a rotating rigid disk supported by isotropic spring is $\alpha\Omega$ in the stationary frame. On the other hand, in the case when the support stiffness (k_t) approaches infinity, only the disk vibratory motion remains effective, for which the theory has been well established.

When the disk has flexibility, equation (15) reduces to, using two-mode approximation in the rotating frame,

$$\begin{aligned}&\{s^{*2} - \mathrm{j}\Omega^*(\alpha - 2)s^* + \omega_t^{*2} + (\alpha - 1)\Omega^{*2}\}(s^{*2} + \omega_{01c}^{*2})(s^{*2} + \omega_{11c}^{*2})\\ &\quad - F_0(s^{*2} + \Omega^{*2})^2(\mathrm{s}^{*2} + \omega_{11c}^{*2}) - F_1(s^{*2} + \Omega^{*2})^2(s^{*2} + \omega_{01c}^{*2}) = 0\end{aligned} \tag{23}$$

or, equivalently in the stationary frame,

$$\begin{aligned}&(s^{*2} - \mathrm{j}\Omega^*\alpha s^* + \omega_t^{*2})(s^{*2} - 2\mathrm{j}\Omega^* s^* - \Omega^{*2} + \omega_{01c}^{*2})(s^{*2} - 2\mathrm{j}\Omega^* s^* - \Omega^{*2} + \omega_{11c}^{*2})\\ &\quad - F_0(s^{*2} - 2\mathrm{j}\Omega^* s^*)^2(s^{*2} - 2\mathrm{j}\Omega^* s^* - \Omega^{*2} + \omega_{11c}^{*2})\\ &\quad - F_1(s^{*2} - 2\mathrm{j}\Omega^* s^*)^2(s^{*2} - 2\mathrm{j}\Omega^* s^* - \Omega^{*2} + \omega_{01c}^{*2}) = 0,\end{aligned} \tag{24}$$

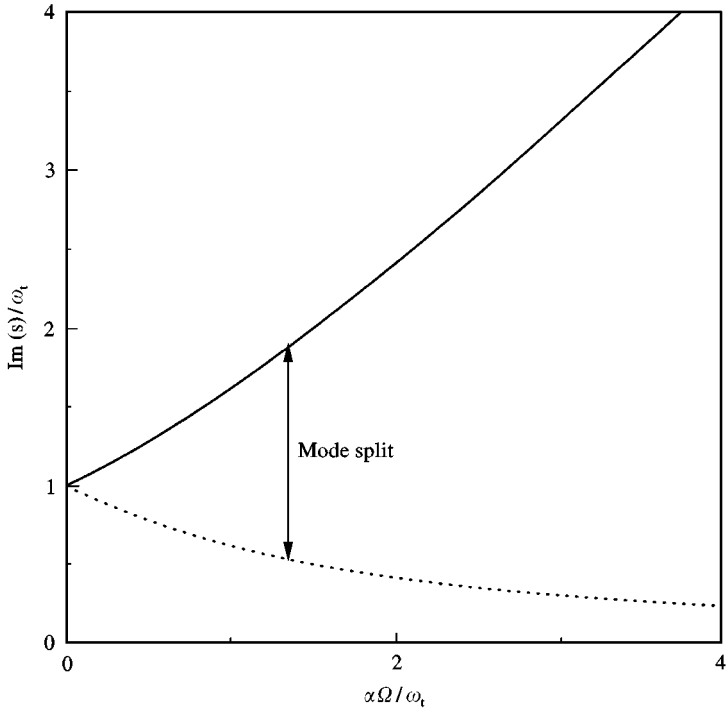

Figure 6. Eigenvalues of a simple rotor supported by isotropic spring [23]: ——: positive; ·····: negative frequency

where the dimensionless parameters are defined as

$$s^* = \frac{s}{\omega_{01}^0}, \quad \Omega^* = \frac{\Omega}{\omega_{01}^0}, \quad \omega_t^* = \frac{\omega_t}{\omega_{01}^0}, \quad \omega_{01c}^* = \frac{\omega_{01c}}{\omega_{01}^0}, \quad \omega_{11c}^* = \frac{\omega_{11c}}{\omega_{01}^0}$$

and ω_{01}^0 is the natural frequency of the non-rotating disk. From equations (23) or (24), we can obtain the modal frequencies of the unbalanced modes for given parameters associated with a multiple disks–shaft system. Since there is no damping, equations (23) or (24) yield six imaginary roots. Also, in the stationary frame,

$$\frac{\Delta\omega_1 + \Delta\omega_2 + \Delta\omega_3}{\Omega} = 6 - \frac{2-\alpha}{1-F_0-F_1} = \left(4 - \frac{2-\alpha}{1-F_0}\right) + \left(2 - \frac{2-\alpha}{1-F_0}\frac{F_1}{1-F_0-F_1}\right), \tag{25}$$

holds, where $\Delta\omega_1$, $\Delta\omega_2$ and $\Delta\omega_3$ are the mode splits associated with the first, second and third forward and backward unbalanced mode pairs respectively. Note that in the stationary frame, the forward modes are larger in absolute frequency than the backward mode. When the single-mode approximation is used, equations (24) and (25), respectively, reduce to

$$(s^{*2} - \mathrm{j}\Omega^*\alpha s^* + \omega_t^{*2})(s^{*2} - 2\mathrm{j}\Omega^* s^* - \Omega^{*2} + \omega_{01c}^{*2}) - F_0(s^{*2} - 2\mathrm{j}\Omega^* s^*)^2 = 0 \tag{26}$$

and

$$2 \leqslant \frac{\Delta\omega_1 + \Delta\omega_2}{\Omega} = 4 - \frac{(2-\alpha)}{1-F_0} < 4 \tag{27}$$

where the inequality relations are proven in Appendix C.

The forward and backward modal frequencies associated with a balanced disk mode are of the same magnitude but reversed in sign when they are defined in the rotating frame. It leads to no mode split, for all balanced disk modes, in the rotating frame but to the mode split of 2Ω in the stationary frame. On the other hand, the mode split associated with the unbalanced mode pairs always occurs for $\alpha \neq 2$, irrespective of the co-ordinates being rotating or stationary. In practice, since we usually observe vibration phenomena of machines and structures with respect to the ground base, it is convenient to express the modal frequencies in the stationary frame for direct comparison with the observations.

5. SIMULATION AND EXPERIMENT

In this section, the numerical simulation for disk vibration was carried out by using the finite element method using annular element [24]. The basic properties of the simulated system are listed in Table 2, which is a typical commercial three-disk HDD spindle system. In Figure 7, the modal frequencies of the three-disk HDD spindle system are shown in the rotating frame. The first unbalanced mode pair (marked 1F and $1\bar{B}$) are lower in absolute frequency than the balanced $(0, 1)$ disk mode pair [marked $(0, 1)$F and $(0, 1)\bar{B}$] where the upper bar means the negative

TABLE 2

Specifications of the three-disk HDD spindle system [22]

	Properties			Dimension (mm)
	Young's modulus (N/m^2)	Poisson's ratio	Density (kg/m^3)	
Hub	$72{\cdot}0 \times 10^9$	0·3	2750	Inner radius = 6·5 Outer radius = 16·5 Length = 10·54
Disk	$72{\cdot}0 \times 10^9$	0·3	2800	Thickness = 0·8 Inner radius = 16·5* Outer radius = 47·5
Yoke	204×10^9	0·3	7800	Bearing properties (refer to Figure 2)
Magnet	$72{\cdot}0 \times 10^9$	0·3	5600	k_{bx} $6{\cdot}0 \times 10^6$ N/m $k_{by} = k_{bz}$ $2{\cdot}0 \times 10^7$ N/m $c_{bx} = c_{by} = c_{bz}$ 0 N s/m

Note: Effective inner radius of 15 mm, considering the imperfect clamping condition, was used in the calculation of the modal parameters of a disk [22].

modal frequency, and F and B denote the forward and backward modes respectively. Note that the unbalanced modes all split in the rotating frame, except when α is equal to 2, as the rotational speed increases unlike the balanced disk modes. While the backward unbalanced modes are larger in absolute frequency than the corresponding forward unbalanced modes in the rotating frame, the reverse holds true in the stationary frame. The results of the two-mode approximation is found to be nearly the same as those of the assumed modes and substructure synthesis method [8], and the single-mode approximation gives fairly good results for the first and second unbalanced modes. Figure 8 shows the same results as in Figure 7 but converted to the stationary frame. Note that the first forward and backward unbalanced modes (marked 1F and $1\bar{B}$) are lower in absolute frequency than the forward and backward balanced (0, 1) disk modes

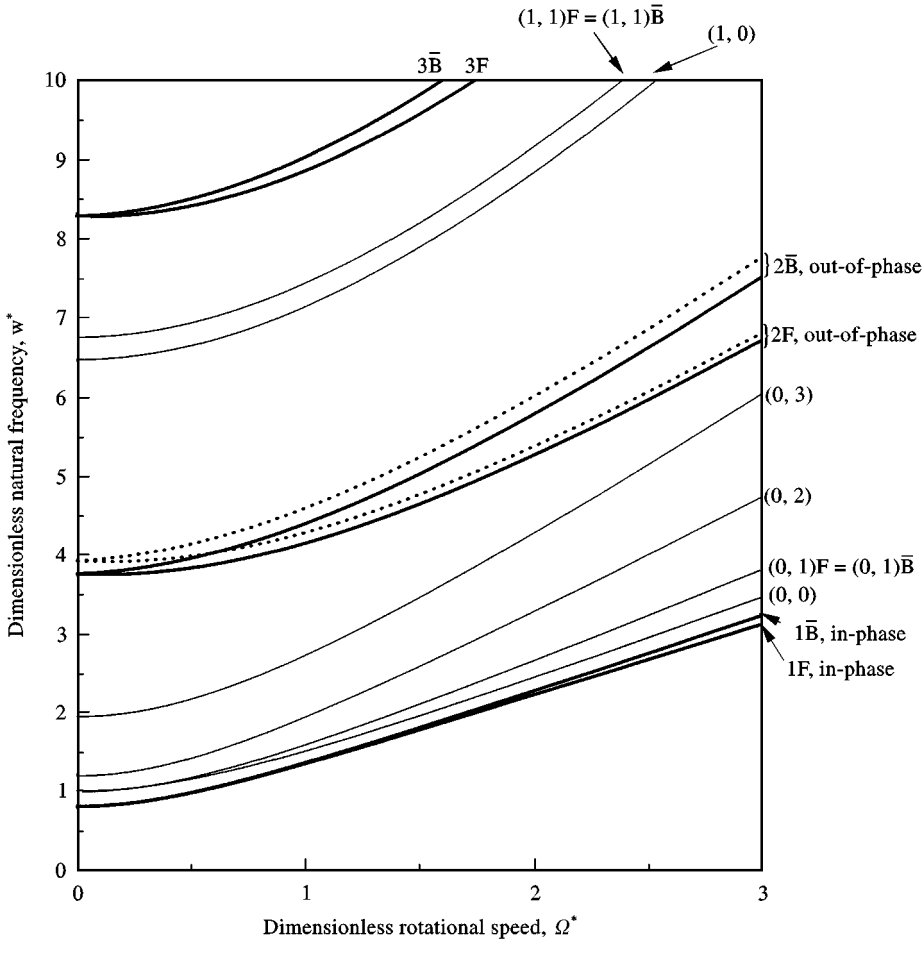

Figure 7. Natural frequencies of HDD spindle system in the rotating frame: $\xi_1 = 0{\cdot}316$, $\omega_t^* = 1{\cdot}33$, $\alpha = 1{\cdot}95$, $\eta = 3{\cdot}62$: - - - -: unbalanced modes (single-mode approximation); ——— : unbalanced modes (two-mode approximation); ——: balanced or disk mode.

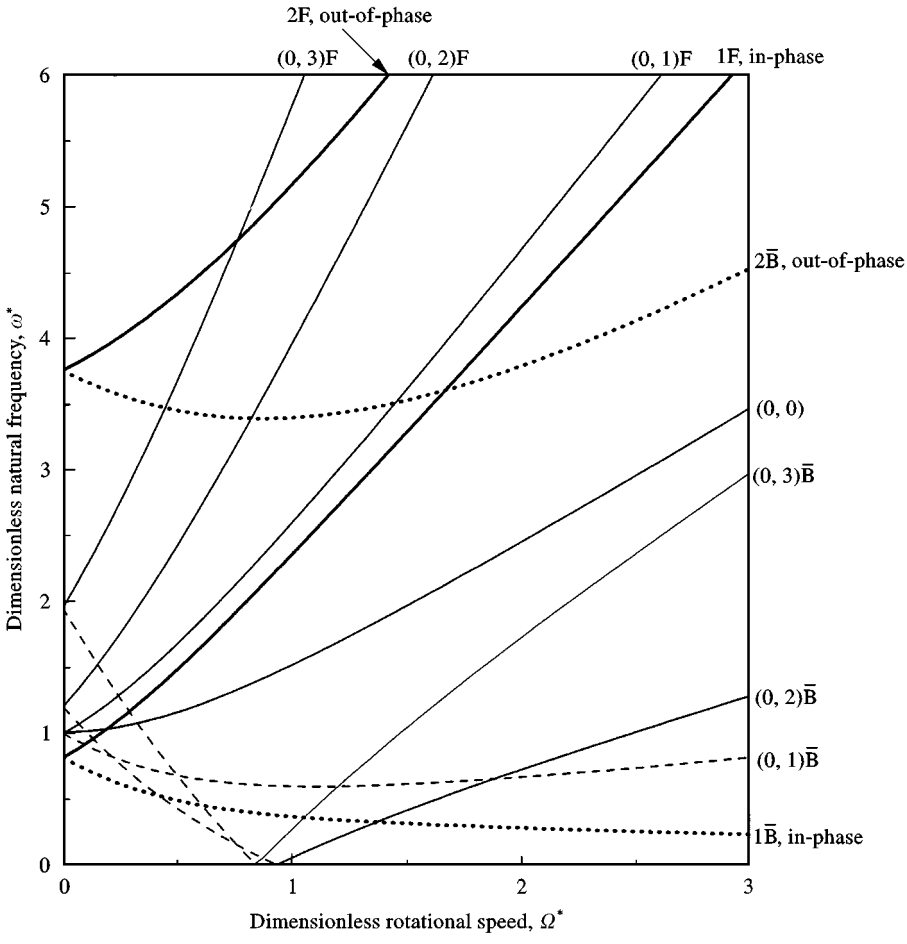

Figure 8. Natural frequencies of HDD spindle system in the stationary frame: $\xi_1 = 0{\cdot}316$, $\omega_t^* = 1{\cdot}33$, $\alpha = 1{\cdot}95$, $\eta = 3{\cdot}62$: ——: forward and backward unbalanced modes (two-mode approx.); – – – –: forward and backward disk modes.

[marked (0, 1)F and (0, 1)$\bar{\text{B}}$], respectively, as in the rotating frame. The mode split at a typical rotational speed of $\Omega^* = 0{\cdot}5$ associated with the first unbalanced mode pair is found to be $1{\cdot}99\Omega$, which is different from, but very close to, 2Ω, the typical mode split associated with the (0, 1) disk mode pair. On the other hand, the mode split at $\Omega^* = 0{\cdot}5$ associated with the second unbalanced mode pair is found to be $1{\cdot}79\Omega$, which is fairly apart from $\alpha\Omega$ ($= 1{\cdot}95\Omega$), the typical mode split associated with free gyro mode pair. In Figure 9, the effects of the coupling factor (η) and the ratio of polar to diametrical moments of inertia (α) on mode split are demonstrated. Note that both η and α tend to significantly influence the split of not the first, but the second, unbalanced mode pair. From this figure, the mode splits of the first and second unbalanced mode pairs at $\Omega^* = 0{\cdot}5$ are found to be $1{\cdot}998\Omega$ and $1{\cdot}89\Omega$ for $\alpha = 1{\cdot}95$ and $\eta = 2{\cdot}5$, $1{\cdot}98\Omega$ and $0{\cdot}90\Omega$ for $\alpha = 1{\cdot}5$ and $\eta = 2{\cdot}5$, and $1{\cdot}99\Omega$ and $1{\cdot}44\Omega$

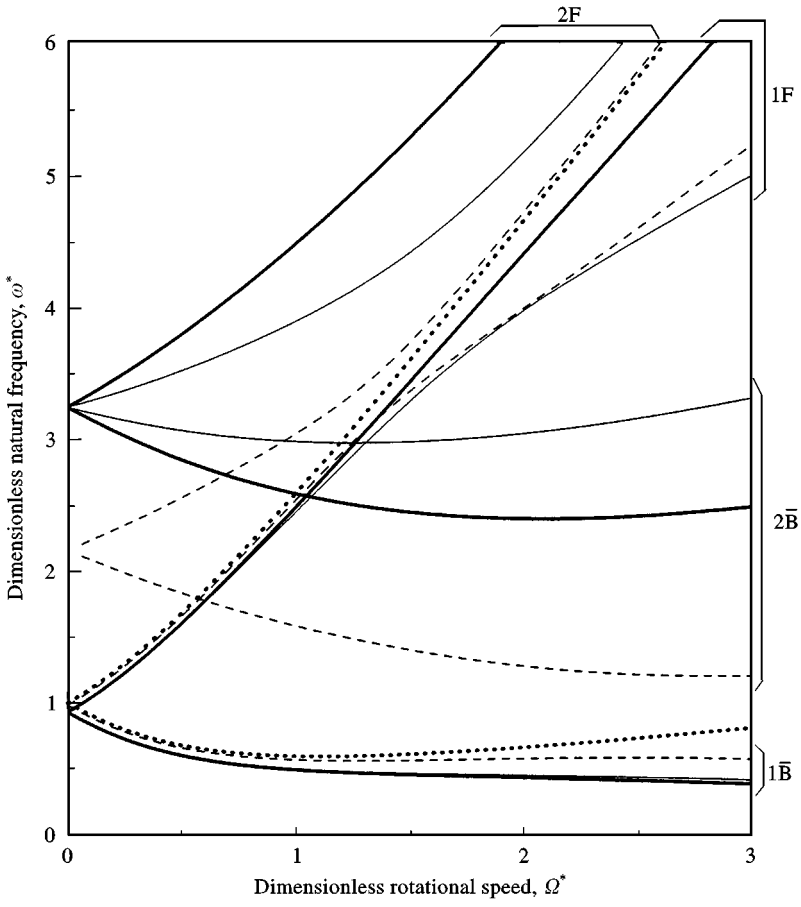

Figure 9. Natural frequencies of bending coupled modes for a disks/shaft system in the stationary frame: $\xi_1 = 0{\cdot}316$, $\omega_t^* = 2$: ——— : $\alpha = 1{\cdot}95$, $\eta = 2{\cdot}5$; ——: $\alpha = 1{\cdot}5$, $\eta = 2{\cdot}5$; – – –: $\alpha = 1{\cdot}5$, $\eta = 0{\cdot}5$; - - - -: balanced (0, 1) disk mode.

for $\alpha = 1{\cdot}5$ and $\eta = 0{\cdot}5$, respectively. In addition, the sums of the two mode splits for each cases are $3{\cdot}89\Omega$, $2{\cdot}88\Omega$ and $3{\cdot}43\Omega$ respectively, which agree well with equation (27). Note that the change in mode split and mean modal frequency due to the coupling effect is noticeable for the second unbalanced mode pair (precession dominant modes), unlike the first unbalanced mode pair which remains nearly the same as the balanced (0, 1) disk mode pair until veering occurs. As the rotational speed increases, the first (marked 1F) and second (marked 2F) forward unbalanced modes approach each other and then veer away. Figure 10 treats the case of weak support ($\omega_t^* = 0{\cdot}5$), in which the mode splits of unbalanced modes are compared with the rigid precessional mode with no coupling. Note that the first unbalanced mode pair are dominated by the rigid-body precessional motion. While the mode split of the first unbalanced mode pair remains nearly as $\alpha\Omega$ (split of rigid disk precessinal mode pair) and that of the second pair decreases due to the coupling effect over the low rotational speed range. Both pairs of unbalanced modes are

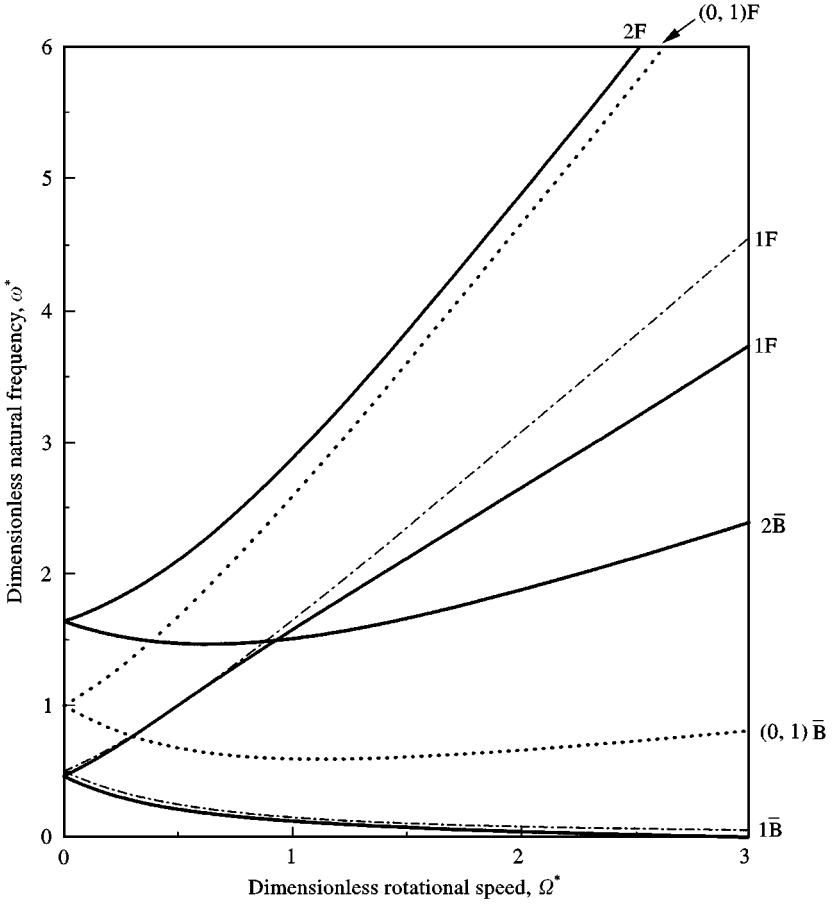

Figure 10. Natural frequencies of bending coupled modes for a disks/shaft system in the stationary frame: $\xi_1 = 0{\cdot}316$, $\omega_t^* = 0{\cdot}5$, $\alpha = 1{\cdot}5$: ——— : unbalanced modes ($\eta = 2{\cdot}5$); – – – – –: rigid precessional modes ($\eta = 0$); - - - -: balanced (0, 1) disk mode.

strongly influenced by the coupling effect over the high rotational speed range. Figure 11 shows the effect of the support stiffness on model splits at $\Omega^* = 0{\cdot}5$. Note that the support stiffness tends to greatly affect the first and second unbalanced mode pairs. The mode split of the first unbalanced mode pair changes from $\alpha\Omega$(free gyro modes) to 2Ω(pure disk modes) as the support stiffness increases. In particular, as the support stiffness changes, the change in mode split associated with the first and second unbalanced mode pairs is pronounced, while the sum of the two mode splits remains nearly unchanged.

From the knowledge of mode splits gained so far, we can easily identify the modes of a multiple disks–shaft system from the so-called waterfall plots. The waterfall plot in Figure 12 was obtained from a series of impact tests with a commercial HDD spindle system fixed on a rigid base [22]. The (0, 2) and (0, 3) disk modes can be easily identified by the degree of mode splits. But, in the frequency range of 450–700 Hz, many modes are densely packed. There appear two

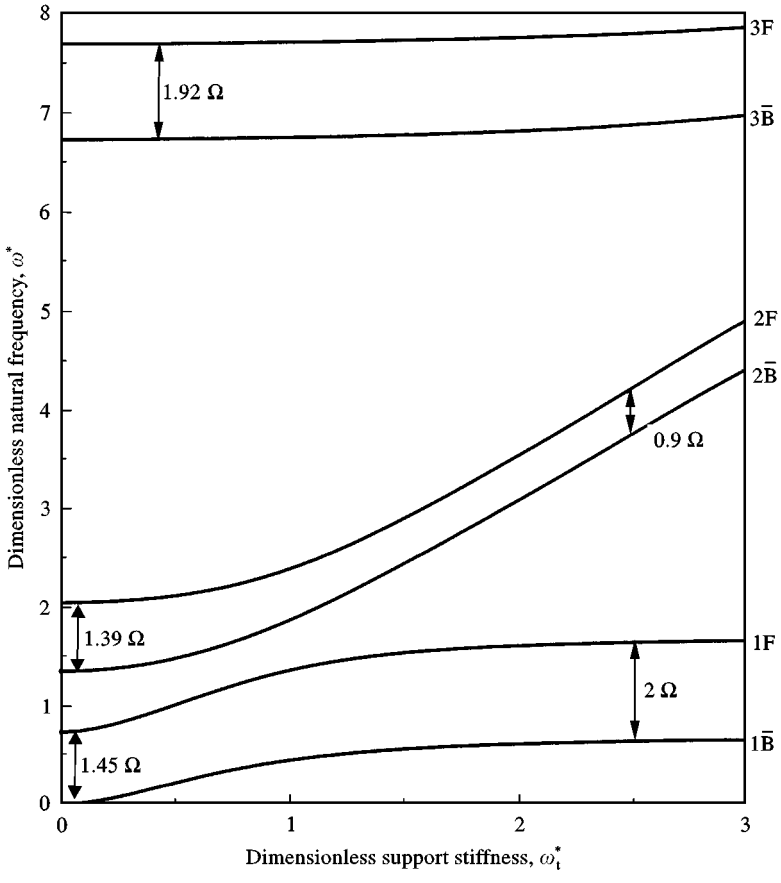

Figure 11. Natural frequencies of bending coupled modes for a disks/spindle system in the stationary frame: $\xi_1 = 0{\cdot}316$, $\alpha = 1{\cdot}5$, $\eta = 2{\cdot}5$,$\Omega^* = 0{\cdot}5$.

pairs of modes with mode split of nearly twice the rotational speed: the pair of lower modes are associated with the first forward (1F) and backward ($1\bar{\mathrm{B}}$) unbalanced modes, and the pair of slightly higher modes are associated with the forward [(0, 1)F] and backward [$(0, 1)\bar{\mathrm{B}}$] balanced disk modes. The second (higher) unbalanced modes did not appear in the frequency range of interest due to the scale limit. The third modal peak with no mode split is associated with either the axial mode or balanced (0, 0) mode.

Summarizing previous discussions, we can simulate the modal frequencies of unbalanced modes over the rotational speed from the characteristic equations (24) or (26), with the proper values of the parameters α, F_0, F_1 and ω_t defined for a multiple disks–shaft system. The first and second unbalanced modal frequencies are always lower and higher in magnitude, respectively, than the balanced (0, 1) disk modes, and the sum of mode splits depends on α, and the coupling factor, but not on the shaft support stiffness. However, the shaft support stiffness affects the mode split of the two lowest unbalanced mode pairs.

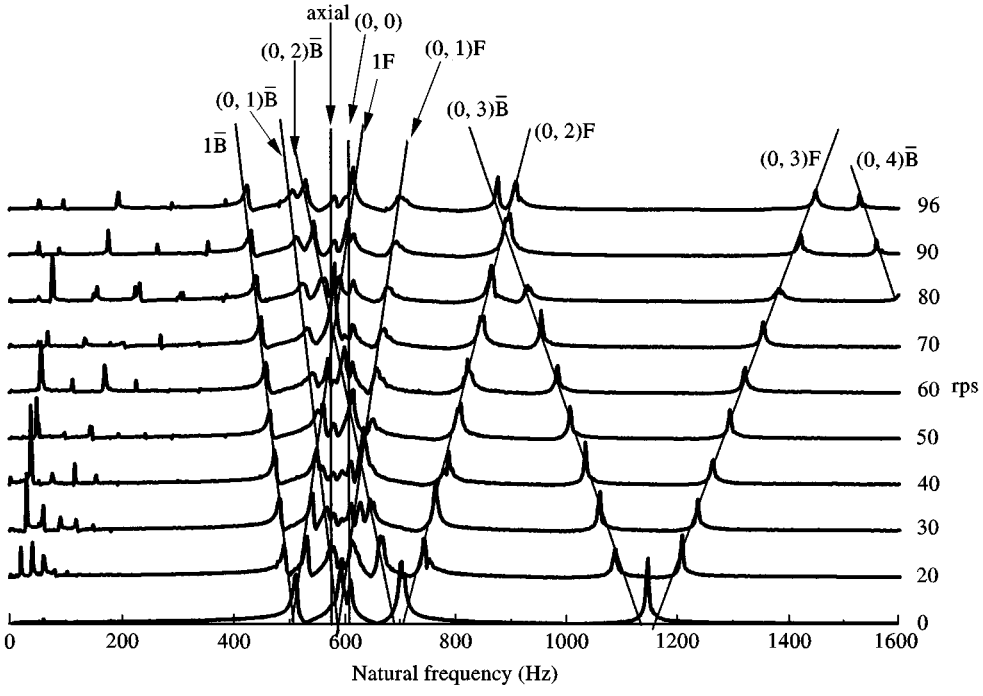

Figure 12. Waterfall plot of the three-disk HDD on a rigid base [22].

6. CONCLUSIONS

The vibrational modes of a multiple disks–shaft system may be easily identified by utilizing the knowledge of their mode splits as the rotational speed changes.

The rotary mode of the rigid shaft and the (0, 1) disk mode are coupled to generate the two unbalanced mode pairs, whose modal frequencies are split in the frequency domain, as the rotational speed changes. The first and second unbalanced modal frequencies are always lower and higher in magnitude, respectively, than the balanced (0, 1) disk modes. The sum of mode splits associated with the two lowest unbalanced mode pairs decreases from $(2 + \alpha)\Omega$ as the coupling factor increases and/or α decreases. The shaft support stiffness determines the mean natural frequencies together with the coupling factor and affects the mode splits of the two lowest unbalanced mode pairs.

For the commercial HDD spindle system with relatively strong support, the decrease in mode split is more pronounced for the second unbalanced mode pair than the first pair, which has nearly the same mode split of 2Ω as the balanced (0,1) disk modes, below the rotational speed where veering occurs. But in the case of weak support, the mode split of the first unbalanced mode pair is nearly the same as $\alpha\Omega$ and, again the decrease in mode split is more pronounced for the second unbalanced mode pair below the rotational speed where veering occurs.

ACKNOWLEDGMENT

This work was partially supported by Samsung Advanced Institute of Technology, Korea.

REFERENCES

1. D. R. Chivens and H. D. Nelson 1975 *ASME Journal of Engineering for Industry* **97**, 881–886. The natural frequencies and critical speeds of a rotating, flexible shaft–disk system.
2. J. A. Dopkin and T. E. Shoup 1974 *ASME Journal of Engineering for Industry*, **96**, 1328–1333. Rotor resonant speed reduction caused by flexibility of disks.
3. F. Wu and G. T. Flowers 1992 *ASME Journal of Vibration and Acoustics* **114**, 242–248. A transfer matrix technique for evaluating the natural frequencies and critical speeds of a rotor with multiple flexible disks.
4. F. J. Wilgen and A. L. Schlack, Jr. 1979 *ASME Journal of Mechanical Design* **101**, 298–303. Effects of disk flexibility on shaft whirl stability.
5. M. Sakata, K. Kimura, S. K. Park and H. Ohnabe 1989 *Journal of Sound and Vibration* **131**, 417–430. Vibration of bladed flexible rotor due to gyroscopic moment.
6. G. T. Flowers and S. G. Ryan 1993 *ASME Journal of Engineering for Gas Turbine and Power* **115**, 227–233. Development of a set of equations for incorporating disk flexibility effects in rotordynamic analyses.
7. A. A. S. Shahab and J. Thomas 1987 *Journal of Sound and Vibration* **114**, 435–452. Coupling effects of disk flexibility on the dynamic behavior of multi disc–shaft system.
8. C. W. Lee and S. B. Chun 1998 *ASME Journal of Vibration and Acoustics* **120**, 87–94. Vibration analysis of a rotor with multiple flexible disks using assumed mode method.
9. H. Lamb and R. V. Southwell 1921 *Proceedings of the Royal Society of London* **99**, 272–280. The vibration of a spinning disk.
10. S. A. Tobias and R. N. Arnold 1957 *Proceedings of the Institute of Mechanical Engineers* **171**, 669–690. The influence of dynamical imperfection on the vibration of rotating disks.
11. C. D. Mote, Jr. 1970 *Journal of the Franklin Institute* **290**, 329–344. Stability of circular plates subjected to moving loads.
12. W. D. Iwan and T. L. Moller 1976 *ASME Journal of Applied Mechanics* **43**, 485–490. The stability of a spinning elastic disk with a transverse load system.
13. Y. Honda, H. Matsushisa and S. Sato 1985 *Journal of Sound and Vibration* **102**, 457–472. Modal response of a disk to a moving concentrated harmonic force.
14. C. J. Radcliffe and C. D. Mote, Jr. 1983 *Journal of Dynamic Systems, Measurement, and Control* **105**, 39–45. Identification and control of rotating disk vibration.
15. C. W. Lee and M. E. Kim 1995 *Journal of Sound and Vibration* **187**, 851–864. Separation and identification of traveling wave modes in rotating disk via directional spectral analysis.
16. J. S. Chen and D. B. Bogy 1992 *ASME Journal of Applied Mechanics* **59**, S230–S235. Effects of load parameters on the natural frequencies and stability of a flexible spinning disk with a stationary load system.
17. C. D. Mote, Jr. 1976 *Journal of the Acoustical Society of America* **61**, 439–447. Moving-load stability of a circular plate on a floating central collar.
18. S. M. Yang 1993 *ASME Journal of Vibration and Acoustics* **115**, 159–164. Vibration of a spinning annular disk with coupled rigid-body motion.
19. J. S. Chen and D. B. Bogy 1993 *ASME Journal of Applied Mechanics* **60**, 471–477. Natural frequencies and stability of a flexible spinning disk-stationary load system with rigid-body tilting.
20. I. Y. Shen and C. -P. R. Ku 1995 *ASME Advances in Information Storage and Processing Systems* ISPS-Vol. 1, 271–282. On the rocking motion of a rotating flexible-disk/rigid-shaft systems.
21. I. Y. Shen and C. -P. R. Ku 1997 *ASME Journal of Applied Mechanics* **64**, 165–169. A nonclassical vibration analysis of a multiple rotating disk and spindle assembly.

22. C. W. Lee, H. S. Jia, J. H. Seo, C. S. Kim, and S. B. Chun 1997 *Sixteenth Biennial ASME Conference on Vibration and Noise, Sacramento, September* Prediction of coupled vibrations in hard disk drive spindle systems
23. C. W. Lee 1993 *Vibration Analysis of Rotors*. Dordrecht: Kluwer.
24. J. Kirkhope and G. J. Wilson 1976 *Journal of Sound and Vibration* **44**, 461–474. Vibration and stress analysis of thin rotating discs using annular finite elements.
25. S. M. Vogel and D. W. Skinner 1965 *ASME Journal of Applied Mechanics* **32**, 926–931. Natural frequencies of transversely vibrating annular plates.

APPENDIX A: EQUATIONS OF MOTION IN THE ROTATING FRAME

$$\int\left[D\nabla^4 w_i - \left\{\frac{h}{r}\frac{\partial}{\partial r}\left(r\sigma_r\frac{\partial w_i}{\partial r}\right) + \frac{h}{r^2}\frac{\partial}{\partial\phi}\left(\sigma_\phi\frac{\partial w_i}{\partial\phi}\right)\right\}\right]\delta w_i r\,\mathrm{d}r\,\mathrm{d}\phi + \int(\ddot{w}_i + \ddot{u}_{ix})\delta w_i\,\mathrm{d}m$$

$$-\int\{r(\ddot{\theta}_y + \Omega^2\theta_y)\sin\phi + r(\ddot{\theta}_z + \Omega^2\theta_z)\cos\phi\}\delta w_i\,\mathrm{d}m = 0,$$

$$(J_2 + \sum_i J_{i2})\ddot{\theta}_y - \{J_1 - J_2 - J_3 + \sum_i (J_{i1} - J_{i2} - J_{i3})\}\Omega\dot{\theta}_z$$

$$+ \{J_1 - J_3 + \sum_i (J_{i1} - J_{i3})\}\Omega^2\theta_y - \sum_i \int r_i(\ddot{w}_i + \Omega^2 w_i)\sin\phi\,\mathrm{d}m_i$$

$$+ c_{br}\{\dot{u}_{oz}(l_2 - l_1) + \dot{\theta}_y(l_1^2 + l_2^2)\} + k_{br}\{u_{oz}(l_2 - l_1) + \theta_y(l_1^2 + l_2^2)\} = 0,$$

$$\left(J_3 + \sum_i J_{i3}\right)\ddot{\theta}_z + \{J_1 - J_2 - J_3 + \sum_i (J_{i1} - J_{i2} - J_{i3})\}\Omega\dot{\theta}_y$$

$$+ \left\{J_1 - J_2 + \sum_i (J_{i1} - J_{i2})\right\}\Omega^2\theta_z - \sum_i \int r_i(\ddot{w}_i + \Omega^2 w_i)\cos\phi\,\mathrm{d}m_i$$

$$+ c_{br}\{\dot{u}_{Gy}(l_2 - l_1) + \dot{\theta}_z(l_1^2 + l_2^2)\} + k_{br}\{u_{Gy}(l_2 - l_1) + \theta_z(l_1^2 + l_2^2)\} = 0,$$

$$\left(M_s + \sum_i M_i\right)\ddot{u}_{Gx} + \sum_i \int \ddot{w}_i\mathrm{d}m_i + 2c_{bx}\dot{u}_{Gx} + 2k_{bx}u_{Gx} = 0,$$

$$\left(M_s + \sum_i M_i\right)(\ddot{u}_{Gy} - 2\Omega\dot{u}_{Gz} - \Omega^2 u_{Gy}) + c_{br}\{2\dot{u}_{Gy} + (l_2 - l_1)\dot{\theta}_z\}$$

$$+ k_{br}\{2u_{Gy} + (l_2 - l_1)\theta_z\} = 0.$$

$$\left(M_s + \sum_i M_i\right)(\ddot{u}_{Gz} + 2\Omega\dot{u}_{Gy} - \Omega^2 u_{Gz}) + c_{br}\{2\dot{u}_{Gz} + (l_1 - l_2)\dot{\theta}_y\}$$

$$+ k_{br}\{2u_{Gz} + (l_2 - l_1)\theta_y\} = 0,$$

where $\theta_z = \partial u_y/\partial x$, $\theta_y = \partial u_z/\partial x$ are Euler angles; indices G, i are the centroid of the system, and the ith disk; u_{ik}, $u_{Gk}(k = x, y, z)$ are the deflections of shaft centerline; J_1, J_2, J_3 the total moment of inertia with respect to x-, y- and z-axis; $J_{in}(n = 1, 2, 3)$ the moment of inertia for the ith disk, M_s, M_i the mass of shaft and disk and, c_{bk}, $k_{bk}(k = r, x, y)$ the damping and stiffness of bearing in each direction.

In-plane stresses due to centrifugal force:

$$\sigma_r = \Omega^2\left(C_1 + \frac{C_2}{r^2} + C_3 r^2\right), \sigma_\phi = \Omega^2\left(C_1 - \frac{C_2}{r^2} + C_4 r^2\right),$$

$$C_1 = \frac{1+v}{8}\rho_d \frac{(v-1)r_1^4 - (3+v)r_2^4}{(v-1)r_1^2 - (1+v)r_2^2},\ C_2 = \frac{1-v}{8}\rho_d r_1^2 r_2^2 \frac{(1+v)r_1^2 - (3+v)r_2^2}{(v-1)r_1^2 - (1+v)r_2^2},$$

$$C_3 = -\frac{3+v}{8}\rho_d,$$

$$C_4 = -\frac{1+3v}{8}\rho_d.$$

APPENDIX B: DIMENSIONLESS EQUATIONS OF DISK MOTION

The equation of motion of the form

$$\frac{Eh^3}{12(1-v^2)}\nabla^4 w_i - \left\{\frac{h}{r}\frac{\partial}{\partial r}\left(r\sigma_r\frac{\partial w_i}{\partial r}\right) + \frac{h}{r^2}\frac{\partial}{\partial\phi}\left(\sigma_\phi\frac{\partial w_i}{\partial\phi}\right)\right\} + \rho_d h\frac{\partial^2 w_i}{\partial t^2} = 0$$

reduces to the dimensionless form of

$$\frac{Eh^2}{12\rho_d(1-v^2)r_2^4}\nabla_\xi^4 w_i - \Omega^2\left\{\frac{1}{\xi}\frac{\partial}{\partial\xi}\left(\xi\sigma_1(\xi)\frac{\partial w_i}{\partial\xi}\right) + \frac{1}{\xi^2}\frac{\partial}{\partial\phi}\left(\sigma_2(\xi)\frac{\partial w_i}{\partial\phi}\right)\right\} + \frac{\partial^2 w_i}{\partial t^2} = 0,$$

$$\nabla_\xi^4 = \left(\frac{\partial^2}{\partial\xi^2} + \frac{1}{\xi}\frac{\partial}{\partial\xi} + \frac{1}{\xi^2}\frac{\partial^2}{\partial\phi^2}\right)^2, \qquad \xi = \frac{r}{r_2}, \qquad \xi_1 = \frac{r_1}{r_2},$$

$$\sigma_1(\xi) = \left(C_1' + \frac{C_2'}{\xi^2} + C_3'\xi^2\right), \qquad \sigma_2(\xi) = \left(C_1' - \frac{C_2'}{\xi^2} + C_4'\xi^2\right),$$

$$C_1' = \frac{1+v}{8}\frac{(v-1)\xi_1^4 - (3+v)}{(v-1)\xi_1^2 - (1+v)}, \qquad C_2' = \frac{1-v}{8}\xi_1^2\frac{(1+v)\xi_1^2 - (3+v)}{(v-1)\xi_1^2 - (1+v)},$$

$$C_3' = -\frac{3+v}{8}, \qquad C_4' = -\frac{1+3v}{8}.$$

Letting $w_i = W(\xi, \phi)f(t)$, we can then formulate the eigenvalue problem given as

$$\frac{1}{\beta_0^4}\nabla_\xi^4 W - \left(\frac{\Omega}{\omega_0}\right)^2\left\{\frac{1}{\xi}\frac{\partial}{\partial\xi}\left(\xi\sigma_1(\xi)\frac{\partial}{\partial\xi}\right) + \frac{1}{\xi^2}\frac{\partial}{\partial\phi}\left(\sigma_2(\xi)\frac{\partial}{\partial\phi}\right)\right\}W = \left(\frac{\omega}{\omega_0}\right)^2 W,$$

where ω_0 is the natural frequency of the non-rotating disk and $\beta_0^4 = 12\rho_d r_2^4(1-v^2)/Eh^2$ is the corresponding dimensionless eigenvalue, which depends on the ratio of the inner to outer radii and the boundary conditions [25]. Thus, the dimensionless modal frequencies and mode shape are dependent upon the dimensionless rotational speed and boundary condition only.

APPENDIX C: INEQUALITY RELATIONS

If we let $R_{01} = const \cdot (\xi - \xi_1)^l,\ l \geqslant 0$, equation (17) yields

$$0 < \frac{H_0(\xi_1)}{1-\xi_1^4} = \frac{[((1-\xi_1)^{l+3}/(l+3)) + 2\xi_1((1-\xi_1)^{l+2}/(l+2)) + \xi_1^2(1-\xi_1)^{l+1}/(l+1)]^2}{(1-\xi_1^4)[((1-\xi_1)^{2l+2}/(2l+2)) + \xi_1(1-\xi_1)^{2l+1}/(2l+1)]}$$

$$\leqslant \frac{1}{4} \quad \text{for } 0 \leqslant \xi_1 < 1. \tag{C1}$$

Note that H_0 approaches the maximum value of 0.25, when $\xi_1 = 0$ and $l = 1$, which coincides with the simulated results in Figures 4 and 5. Since H_m for higher modes are much smaller than H_0 as shown in Figure 4, the relation (C1) holds true for the higher modes. On the other hand, we can derive the relation from equations (18) and (19) as

$$\chi_2 = \frac{\alpha}{\eta}\frac{\pi\rho_d h r_2^4}{J_p^d} - 1 = \frac{\alpha}{\eta}\frac{2r_2^4}{r_2^4 - r_1^4} - 1 = \frac{2\alpha}{\eta(1-\xi_1^4)} - 1. \tag{C2}$$

Since $\chi_2 \geqslant 0$ by definition, equation (C2) yields

$$0 < \eta \leqslant \frac{2\alpha}{1-\xi_1^4}. \tag{C3}$$

From equations (16), (C1) and (C3), we obtain

$$0 < F_0 = \eta \mathrm{H}_0(\xi_1) \leqslant \frac{2\alpha H_0(\xi_1)}{1-\xi_1^4} \leqslant \frac{\alpha}{2} \tag{C4}$$

and

$$0 < \frac{2-\alpha}{1-F_0} \leqslant \frac{2-\alpha}{1-\alpha/2} = 2. \tag{C5}$$